Korean J. Chem. Eng., 33(11), 3222-3230 (2016)
DOI: 10.1007/s11814-016-0180-9

pISSN: 0256-1115
eISSN: 1975-7220

CO_2 absorption characteristics of a piperazine derivative with primary, secondary, and tertiary amino groups

Jeong Ho Choi*,, Young Eun Kim*, Sung Chan Nam*, Soung Hee Yun*, Yeo Il Yoon*,†, and Jung-Hyun Lee****

*Green Energy Process Laboratory, Climate Change Research Division, Korea Institute of Energy Research, 152, Gajeong-ro, Yuseong-gu, Daejeon 34129, Korea
**Department of Chemical & Biological Engineering, Korea University, 5-1 Anam-dong, Seongbuk-gu, Seoul 02841, Korea
(*Received 25 March 2016 • accepted 24 June 2016*)

Abstract−Thermodynamic and kinetic data are important for designing a CO_2 absorption process using aqueous amine solutions. A piperazine derivative, 1-(2-aminoethyl)piperazine (AEP), was blended with aqueous amine solutions due to its thermal degradation stability, high CO_2 loading (mole of CO_2-absorbed per mole of amine) and high solubility in water. In this study, the vapor liquid equilibrium (VLE), absorption rate, and species distribution of aqueous AEP solutions were studied to develop an optimum amine solution in a post-combustion capture process. The VLE and apparent absorption rate of the aqueous 30 wt% AEP solution were measured using a batch-type reactor at 313.15, 333.15, and 353.15 K. The AEP exhibited approximately twice higher CO_2 loading compared with monoethanolamine (MEA) at all temperatures. The apparent AEP absorption rate (k_{app}=0.1 min^{-1}) was similar to that of diethanolamine (DEA) at 333.15 K. Speciation of the CO_2-absorbed AEP was analyzed using ^{13}C NMR. Although AEP featured a primary amino group and secondary amino group, it did not form bicarbamate upon reaction with CO_2 based on analysis results. AEP-1-carbamate was primarily formed by reactions between AEP and CO_2 during the initial reaction. Bicarbonate species formed as the quantity of absorbed CO_2 increased.

Keywords: Carbon Dioxide, CO_2 Absorption, Piperazine Derivatives, Vapor Liquid Equilibrium, CO_2 Apparent Absorption Rate

INTRODUCTION

As the greenhouse gas concentration increases in the atmosphere, various problems caused by global climate change are arising globally [1]. Carbon dioxide (CO_2), one of the six major greenhouse gases, can be controlled through carbon capture and storage (CCS) technologies. CO_2 capture technologies can be classified into three categories: pre-combustion, post-combustion, and oxy-fuel combustion [2,3]. Absorption (wet or dry systems), adsorption, membranes, cryogenics, hydrates, and other processes have been studied for CO_2 separation and capture from flue gas, and each process has advantages and disadvantages [4,5].

Studies on CO_2 absorption have been conducted for various aspects, such as absorption capacity, absorption rate, reaction heat, degradation of absorbent, and corrosion [6-9]. Monoethanolamine (MEA), which is widely used in commercial processes, exhibits a faster reaction rate with CO_2 than other alkanolamine absorbents, such as diethanolamine (DEA), methyldiethanolamine (MDEA), and 2-amino-2-methyl-1-propanol (AMP). However, the manufacturing and operating costs of MEA processes can be increased due to various disadvantages, such as a high absorbent makeup rate through thermal and oxidative degradation and vaporization, high corrosion of equipment, low absorption capacity, and high regeneration energy required for absorbent regeneration at the desorber [10,11]. Many researchers have attempted to improve CO_2 absorption performance over conventional alkanolamines [12,13]. Enhancements were achieved from developing materials and processes. Several researchers have focused on studying materials, including synthesized absorbents and blended absorbents. Other researchers studied design, operation, and optimization of the processes. In addition, degradation, corrosion and their inhibitors have been studied to successfully operate the process at a low cost [14-17].

Recently, an aqueous 1-(2-aminoethyl)piperazine (AEP) solution emerged as a new absorbent; AEP is a cyclic amine that includes a primary, a secondary, and a tertiary amino group in a molecule. The AEP molecule exhibits desirable physical properties, such as a high boiling point (491.15-495.15 K), low vapor pressure (0.05 hPa at 295.15 K) and good solubility in water (fully miscible). Several researchers have demonstrated the advantages of an aqueous AEP solution compared with conventional amines (MEA, DEA, MDEA etc.). Du et al. [18] proposed that a novel blend of piperazine (PZ) with AEP exhibited superior absorbency for CO_2 capture [18]. Aqueous PZ/AEP showed high CO_2 loading and stable degradation resistance without the precipitation problem of highly concentrated PZ. Du and Rochelle [19] studied a thermodynamic model in the framework of electrolyte nonrandom two-liquid (eNRTL) activity coefficient model to predict CO_2 loading, speciation and volatility for an aqueous PZ/AEP solution. The heat of reaction for

†To whom correspondence should be addressed.
E-mail: 21yoon@kier.re.kr
‡This article is dedicated to Prof. Sung Hyun Kim on the occasion of his retirement from Korea University.

6 m AEP (50-70 kJ/mol CO_2) was less than 5 m PZ/2 m AEP (75-85 kJ/mol CO_2) [19]. Rate constants, VLE and other physical data are used to improve mathematical models for CO_2 absorption processes [20,21]. Furthermore, the improved models can elucidate the treated systems and, thereby, increase confidence in the proposed technological concept [20].

In this study, the absorption capacity, absorption rate, and absorption mechanism of CO_2 in an aqueous AEP solution were investigated because only limited information on the AEP solution CO_2 absorption exists. CO_2 loading and apparent absorption rate of the AEP solution were measured using a vapor liquid equilibrium (VLE) apparatus to evaluate the CO_2 absorption performance, and the results were compared with MEA, which is a representative commercialized absorbent. In addition, the species distributions between CO_2 and absorbent were analyzed using nuclear magnetic resonance (NMR) and mass spectrophotometry (MS). Verifying the species is important for understanding the absorbents' characteristics [22,23].

REACTION MECHANISM

The AEP includes primary, secondary, and tertiary amino groups in the molecule. Therefore, it was expected to show all the CO_2 absorption characteristics of primary, secondary, and tertiary amines. The single amine CO_2 absorption mechanisms are presented in the following sections, 1 and 2, to clarify the AEP characteristics.

1. Primary and Secondary Amines

The amine and CO_2 reaction mechanism has been studied by various researchers [24-29]. Kenig et al. [29] presented an overview of the CO_2 absorption mechanism for primary (RNH_2), secondary (R_2NH), and tertiary amines (R_3N) [29]. The reaction mechanisms between CO_2 and alkanolamines (primary and secondary) were originally proposed by Caplow [24] and Danckwerts [25]. Danckwerts [25] explained that two molecular reactions form a zwitterion; and the zwitterion becomes a carbamate as protons are eliminated by a base (B), such as RNH_2, H_2O. This CO_2 absorption mechanism comprises the following two steps.

$$CO_2+RNH_2 \leftrightarrow RNH_2^+COO^- \quad (1)$$

$$RNH_2^+COO^- + B \leftrightarrow RNHCOO^- + BH^+ \quad (2)$$

The zwitterion mechanism was validated through molecular modeling, and Xie et al. [26] measured the CO_2 absorption reaction of an aqueous primary amine solution [26]. A polarizable continuum model and a micro-kinetic model were used to confirm an intermediate in the system. Based on the previous studies, primary and secondary amines formed a carbamate intermediate for CO_2 reaction.

The overall reaction for primary and secondary amines with CO_2 is as follows.

$$CO_2+RNH_2+B \leftrightarrow RNHCOO^- + BH^+ \quad (3)$$

2. Tertiary Amine

Tertiary amines feature high absorption capacity, low regeneration energy, and high degradation stability. The tertiary amine reacts with CO_2, which only forms bicarbonate species. Absorbents that form bicarbonate species feature a lower regeneration energy and higher absorption capacity than primary and secondary amine-forming carbamate species. Barzagli et al. [30] studied CO_2 absorption and desorption for the DEA and MDEA, which showed that the tertiary amine, MDEA, was more stable against degradation than the secondary amine, DEA [27]. The overall reaction of the tertiary amine with CO_2 is selective formation of bicarbonate, as represented in Eq. (4).

$$R_1R_2R_3N+CO_2+H_2O \leftrightarrow R_1R_2R_3NH^+ + HCO_3^- \quad (4)$$

As mentioned above, amino groups and CO_2 exhibit different intermolecular interactions. Numerous studies have used NMR analyses to investigate primary, secondary and tertiary amines and verify the CO_2 absorption mechanism [30,31]. In addition, different types of amines were mixed, and their characteristics were reviewed.

EXPERIMENTAL

The reagents, AEP (purity: 99%) and MEA (purity: 98%), were obtained from Sigma-Aldrich. Each reagent was used without further refinement and mixed with deionized water at a 30 wt% concentration.

1. Vapor Liquid Equilibrium

A VLE apparatus equipped with a magnetic stirrer was used to measure the CO_2 pressure over time. The data were used to calculate the CO_2 loading (mole of CO_2 absorbed per mole of amine) and apparent absorption rate. The apparatus configuration is shown in a previously published paper [32], and CO_2 (99.99 vol%) was used as the feed gas for the VLE apparatus.

The reservoir was filled with CO_2 and preheated to 313.15 K in a water bath prior to supplying the reactor, and the experiments were conducted in the reactor at 313.15, 333.15 and 353.15 K, respectively. A K-type thermocouple was used to measure the internal temperatures of the reservoir and reactor. A pressure sensor, PSHFC model (range: −1-10 kg_f/cm^2) from Sensys with the precision 0.001 kg_f/cm^2 was used to measure the reservoir and reactor gas pressures. One hundred milliliters of absorbent was supplied to each reactor. After the absorbent was injected into the reactor, the reactor was connected to a vacuum pump to remove residual gas, and CO_2 gas was injected into the reactor after reaching a constant reactor temperature.

In addition, the absorbent was stirred at a constant rate of 170 rpm to maximize the effective interfacial area of CO_2 and absorbent and minimize the surface resistance of mass transfer. The reactor pressure decreased with the CO_2 pressure as the reaction proceeded, and the reaction reached an absorption equilibrium when the pressure deviation was constant for more than 1 hour. The CO_2 equilibrium partial pressure was computed by measuring the pressure when equilibrium was reached, and CO_2 was added to the reactor after it reached the first equilibrium. This process was repeated several times until the maximum saturation point was reached and no more CO_2 could be absorbed.

2. Nuclear Magnetic Resonance Spectroscopy

Nuclear magnetic resonance spectroscopy, Avance 500 MHz from Bruker, was used to identify the absorbent species. Deute-

rium oxide (D_2O) (99.99%) was used as the solvent for the NMR measurements and was purchased from Sigma-Aldrich, and 1.4-dioxane was used as an external reference for the ^{13}C NMR analyses. The 1.4-dioxane peaks were observed at δ=67.0 ppm in the ^{13}C NMR spectrum. The absorbent species distribution was analyzed based on the change in CO_2 loading.

3. Mass Spectroscopy

Mass spectroscopy (MS) and NMR were used to confirm the absorbent species distribution. The absorbent sample was diluted 1000-fold with deionized water and directly infused into an MS instrument (LCQ Deca XP Plus from Thermo Scientific) using the following parameters: infusion flow rate (3 L/min), electrospray voltage (5.0 kV), capillary temperature (548.15 K), and capillary voltage (15 V). Zoom scans, MS/MS scans, and MS/MS/MS scans were acquired for the ions of interest. For the MS/MS or MS/MS/MS analyses, collision-induced dissociation (CID) with a normalized collision energy of 35% was used.

RESULT AND DISCUSSION

1. Vapor Liquid Equilibrium

The equilibrium partial pressure of CO_2 ($P^*_{CO_2}$) within the reactor was calculated by subtracting the initial pressure (P^0) from the equilibrium pressure (P^*) upon absorption equilibrium, as delineated in Eq. (5).

$$P^*_{CO_2} = (P^* - P^0) \tag{5}$$

As shown in Eq. (6), moles of injected CO_2 are computed by subtracting the pressure of the reservoir, after the CO_2 has been injection into the reactor, from the initial pressure of the reservoir, and multiplying the difference by the volume of the reservoir and dividing the product of the multiplication by RT. As shown in Eq. (7), moles in the gas of the reactor, when the equilibrium has been reached, are computed by subtracting the initial pressure of the reactor, which is a vacuum, from the final pressure of the reactor and multiplying the difference by the volume of the gas, and dividing the product of the multiplication by RT, and then finally applying the resulting value into the ideal gas equation. It was assumed that CO_2 behavior as an ideal gas in the VLE experiments. The moles of absorbed CO_2 in the absorbent can be calculated by the Eq. (8).

$$n_{S_{CO_2}} = \frac{(P_{Si} - P_{St}) \times V_S}{RT_S} \tag{6}$$

$$n_{R_{CO_2}} = \frac{(P_{Ri} - P_{Rt}) \times V_R}{RT_R} \tag{7}$$

$$n_{absorbed_{CO_2}} = n_{S_{CO_2}} - n_{R_{CO_2}} \tag{8}$$

The quantity of chemically absorbed CO_2 in the absorbent can be represented by CO_2 loading, which is the moles of absorbed CO_2 per mole of amine and is expressed as Eq. (9).

$$CO_2 \text{ loading} = \frac{n_{absorbed_{CO_2}}}{n_{amine}} \tag{9}$$

The apparent absorption rate (k_{app}) for CO_2 can be calculated using Eqs. (10), (11) [33], which was calculated as half of the final time ($t_{1/2}$).

$$\ln(P_{CO_2(1/2)} - P^*_{CO_2}) = -K_{app} \cdot t + C \tag{10}$$

$$K_{app} = \frac{-\ln[(P_{CO_2(1/2)} - P^*_{CO_2})/(P^0_{CO_2} - P^*_{CO_2})]}{t_{1/2}} \tag{11}$$

For Eq. (10), C is the difference between the initial CO_2 pressure ($P^0_{CO_2}$) and equilibrium pressure ($P^*_{CO_2}$) of the reactor. The apparent absorption rate was computed with respect to the point at which the pressure dropped to half of the equilibrium pressure ($P_{CO_2(1/2)}$).

The apparent absorption rate for the amine and CO_2 followed a pseudo-first-order reaction.

For the MEA, CO_2 loading was limited to α=0.60 (mol CO_2/mol MEA) at 333.15 K, whereas AEP showed high CO_2 loading at α=1.27 (mol CO_2/mol AEP) for the same temperature. The relationship between CO_2 loading and equilibrium partial pressure of CO_2 is illustrated in Fig. 1. In contrast to the data from Choi et al. [34], the apparent absorption rate for AEP was similar to DEA [34]. Each CO_2 loading and apparent absorption rate is listed in Table 1. As Fig. 2 shows, the AEP absorption rate of AEP is slower than MEA and is similar to DEA and AEP. For AEP, the CO_2 loading was approximately twice greater than MEA at all temperatures, and AEP exhibited excellent CO_2 absorption characteristics for the CO_2 loading and absorption rate. AEP also exhibited high stability against thermal degradation compared with MEA [18]. Therefore, AEP can likely replace MEA as an absorbent. Furthermore, the results can be applied to predict a process design model.

2. Speciation

2-1. Nuclear Magnetic Resonance Spectroscopy

When an excited nucleus returns to the ground state, the process is referred to as relaxation. Spin-lattice relaxation and spin-spin relaxation are detected through NMR, and each arises through a first-order rate process and can be characterized by the relaxation time that dominates the dissipation rate. Ciftja et al. [35] revealed that a sufficient relaxation time is important for determining the

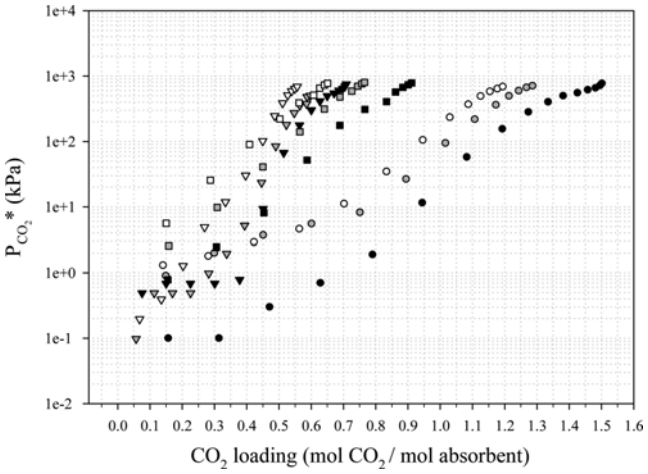

Fig. 1. VLE between CO_2 and aqueous 30 wt% amine solution. Circle: AEP solution; quadrangle: MEA solution; and inverted triangle: DEA [34] solution, black: 313.15 K, gray: 333.15 K, and white: 353.15 K.

Table 1. CO_2 loading and apparent absorption rate of aqueous AEP solutions at 313.15, 333.15, and 353.15 K

	CO_2 loading (mole CO_2/mole amine)			Apparent absorption rate, k_{app} (min^{-1})		
	313.15 K	333.15 K	353.15 K	313.15 K	333.15 K	353.15 K
MEA	0.71	0.60	0.56	0.12	0.24	0.35
DEA [34]	0.91	0.77	0.65	0.08	0.10	0.12
AEP	1.50	1.29	1.20	0.05	0.10	0.16

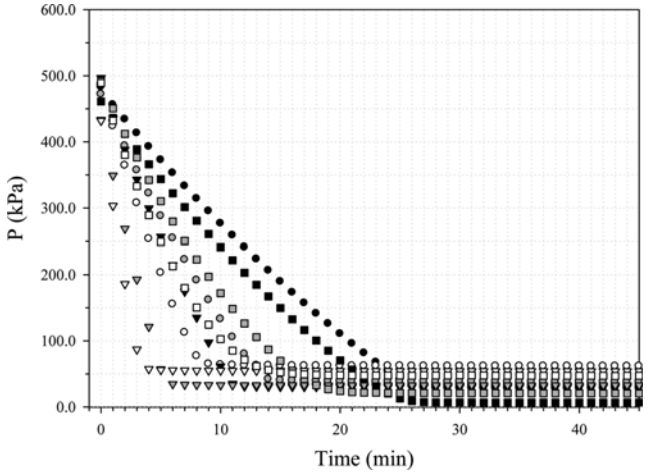

Fig. 2. Absorption rate of CO_2 into aqueous 30 wt% amine solutions. Circle: AEP solution; quadrangle: DEA [34] solution; and inverted triangle: MEA solution, black: 313.15 K, red: 333.15 K, and green: 353.15 K.

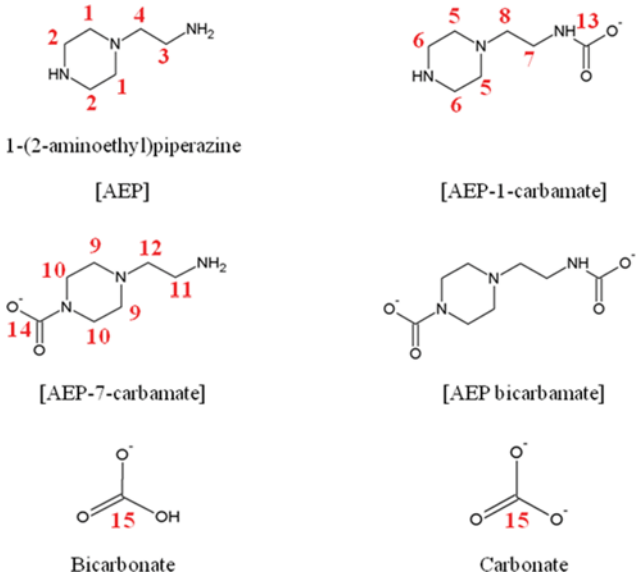

Fig. 3. Molecular structures of species in the CO_2-absorbed aqueous AEP solution.

Table 2. NMR analysis parameters at room temperature (298.15 K)

		^{1}H NMR	^{13}C NMR
Analysis parameter	Number of scans	32	64
	Acquisition time	3.172 s	1.091 s
	Relaxation delay time	1 s	60 s
	Dwell time	48.4 μs	16.65 μs

magnitude (intensity) of the peaks in NMR. Pulse D1=~5-6×T1 (D1: relaxation delay time, T1: relaxation time), and NS=300 (NS: number of scans) have been proposed for using the inverse gated decoupling method [35]. Therefore, we measured the ^{13}C NMR relaxation time prior to the experiment to determine the relax-

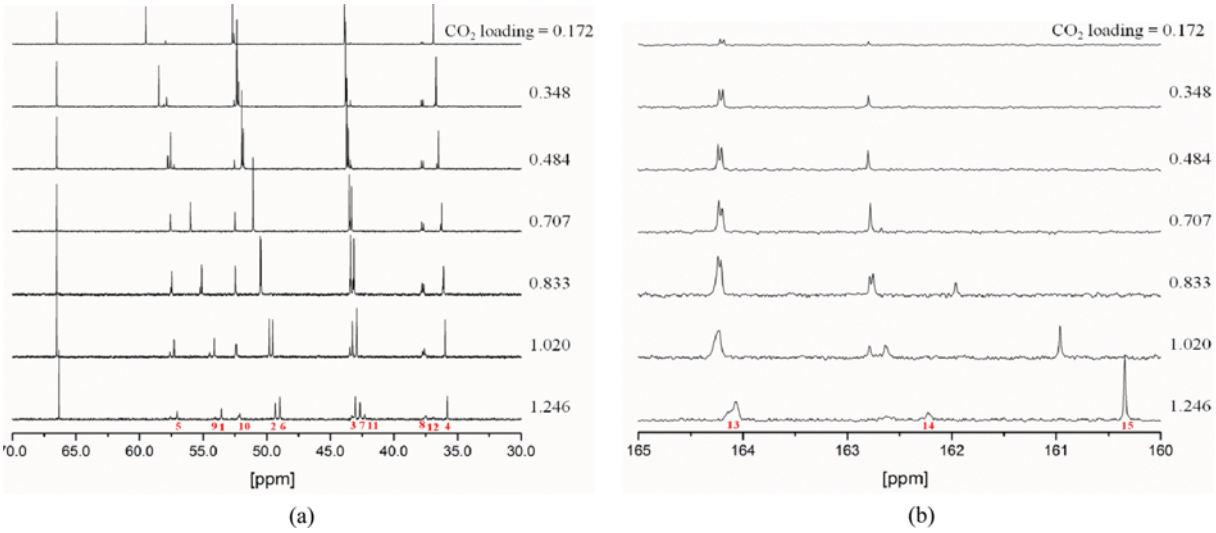

Fig. 4. ^{13}C NMR spectra of the AEP-H_2O-CO_2 system at 333.15 K; (a) high field and (b) low field.

Table 3. Chemical shifts in the AEP ^{13}C NMR spectra at 333.15 K

	Peak location, δ (area)														
	Free AEP				AEP-1-carbamate					AEP-7-carbamate					Carbonate bicarbonate
CO_2 loading	1	2	3	4	5	6	7	8	13	9	10	11	12	14	15
0.172	59.49 (1.00)	52.70 (1.96)	43.86 (1.81)	36.89 (1.03)	57.95 (0.15)	52.55 (overlap)	43.39 (overlap)	37.72 (0.15)	164.18 (0.14)					162.80 (0.04)	
0.348	58.47 (0.99)	52.34 (1.96)	43.78 (1.93)	36.67 (1.00)	57.86 (0.38)	52.21 (0.76)	43.71 (0.80)	37.71 (0.36)	164.19 (0.41)	58.13 (0.08)	52.56 (0.19)	43.41 (0.19)	36.80 (0.08)	162.79 (0.15)	
0.484	57.56 (1.16)	51.95 (2.09)	43.69 (2.04)	36.49 (1.00)	57.77 (0.57)	51.85 (1.30)	43.58 (1.29)	37.69 (0.32)	164.20 (0.66)	57.29	52.53 (0.39)	43.42 (0.32)	36.61 (0.15)	162.80 (0.22)	
0.707	56.00 (1.00)	51.07 (overlap)	43.51 (2.05)	36.21 (1.00)	57.58 (1.18)	51.07 (overlap)	43.32 (2.30)	37.66 (1.01)	164.19 (1.23)	55.96 (overlap)	52.47 (0.97)	43.44 (overlap)	36.34 (0.35)	162.77 (0.51)	162.67 (0.08)
0.833	55.10 (1.00)	50.50 (2.11)	43.39 (2.10)	36.08 (overlap)	57.45 (1.07)	50.43 (2.13)	43.13 (2.17)	37.64 (1.08)	164.20 (1.59)	55.23 (0.70)	52.45 (1.42)	43.21 (0.73)	36.08 (overlap)	162.75 (0.73)	161.95 (0.24)
1.020	54.10 (0.77)	49.78 (1.69)	43.24 (1.56)	35.96 (overlap)	57.28 (0.76)	49.54 (1.53)	42.91 (2.38)	37.60 (0.70)	164.22 (1.27)	54.48 (0.60)	52.38 (1.25)	43.46 (0.44)	35.96 (overlap)	162.63 (0.41)	160.96 (0.55)
1.246	53.69 (0.61)	49.46 (1.30)	43.18 (1.16)	37.03 (overlap)	57.20 (1.07)	49.46 (overlap)	42.81 (1.10)	37.62 (0.62)	164.21 (0.91)	54.21 (0.26)	52.26 (0.43)	42.42 (0.42)	37.03 (overlap)	162.37 (0.27)	160.49 (0.98)

ation time required for the analysis. A longer time period than the relaxation time is necessary to measure ^{13}C NMR, and a quantitative analysis of the experiments provided inaccurate information. Therefore, we selected analytical conditions based on prior experiments and published papers. The ^{13}C NMR analytical conditions used in the experiment are listed in Table 2. In addition, we measured two-dimensional (2D) NMR to discern interactions due to long range coupling of AEP, but no long range coupling occurred. Preliminary research showed that the quantitative ^{13}C NMR analysis would verify the species' behavior; AEP verified the behavior through ^{13}C NMR based on numerous overlapping ^{1}H NMR phenomena. The species that formed as the reaction proceeded are illustrated in Fig. 3. The location can be determined using Fig. 4, and more detailed locations are listed in Table 3. The AEP-1-carbamate peak manifested at a high field (δ=36.89-37.03 ppm) and a low field (δ=164.18-164.21 ppm), which is illustrated in Fig. 4. Primary amines were expected to be noticeably active during the initial phase of the reaction, and, as predicted, AEP-1-carbamate formation was observed during the initial phase of the reaction. This research is based on quantitative ^{13}C NMR, and the relative quantity of carbamate formed at the low field was verified, which showed that the quantity of AEP-7-carbamate increased as the reaction proceeded. The increase in AEP-1-carbamate and AEP-7-carbamate was minimal at α=0.71 (CO_2 loading), and bicarbonate-type spe-

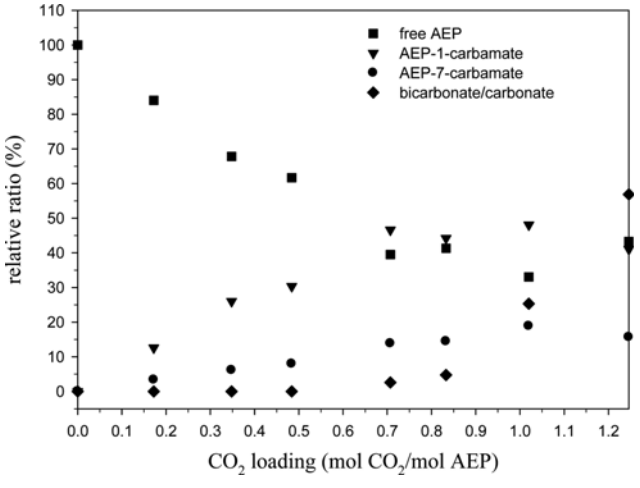

Fig. 5. Species distribution for AEP 30 wt% at 333.15 K. Symbols. Quadrangle: free AEP; Inverted triangle: AEP-1-carbamate; Circle: AEP-7-carbamate; diamond: bicarbonate/carbonate.

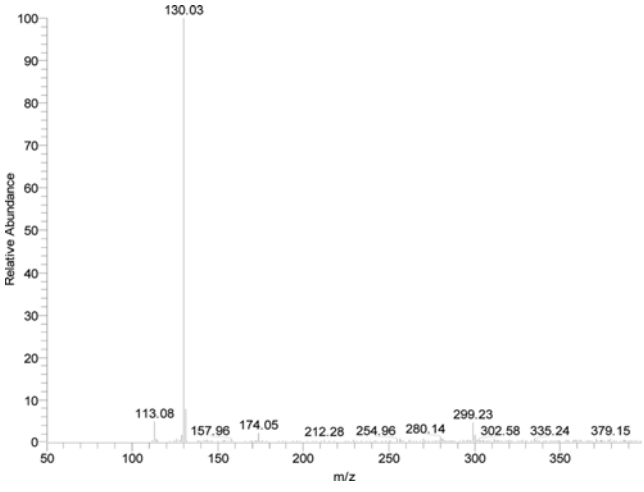

Fig. 6. MS spectrum for a CO_2-saturated AEP solution.

cies were formed. When primary, secondary, and tertiary amino groups were mixed, the results show that the reactivity of the primary amine was most apparent and the reactions occurred in the order of secondary and tertiary functional groups as the reaction proceeded. The related species distribution ratio was calculated from the integrated value for the ^{13}C NMR quantity and detailed species distribution for the AEP and CO_2 reaction shown in Fig. 5.

2-2. Mass Spectrometry

MS and ^{13}C NMR were used to verify the species expected in the absorbents. The MS spectrum of CO_2-saturated AEP is shown in Fig. 6; the 100-400 mass to charge ratio (m/z) scan method was used. The expected molecular weights are as follows: AEP=129.2, protonated AEP $[AEP+H]^+$=130.2, AEP carbamate $[AEP+CO_2+H]^+$ =174.2, and $[AEP-NH_3+H]^+$=113.2. AEP carbamate was also observed in the ^{13}C NMR high field. But, AEP bicarbamate, the formation of which was expected as two CO_2 molecules were attached to AEP, did not form based on the MS spectra (molecular weight of $[AEP+2CO_2+H]^+$=218.2). Materials observed in the MS spec-

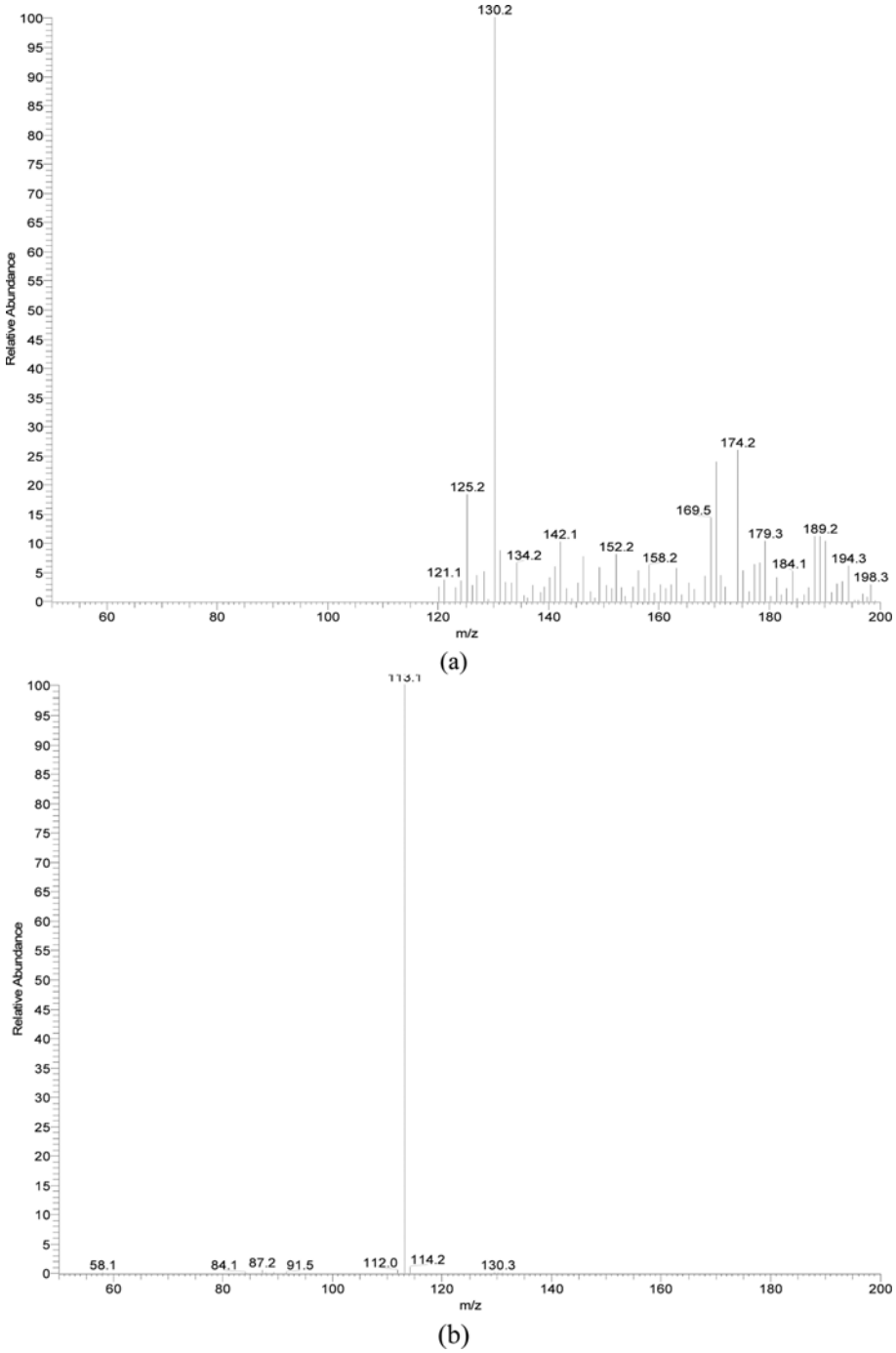

Fig. 7. Separation patterns of free AEP in a CO_2-saturated AEP solution: (a) $[AEP+H]^+$=130.2 (MS), (b) $[AEP-NH_3+H]^+$=113. 0 (MS/MS) and (c) $[AEP-NH_3-CO_2+H]^+$=84.1 (MS/MS/MS).

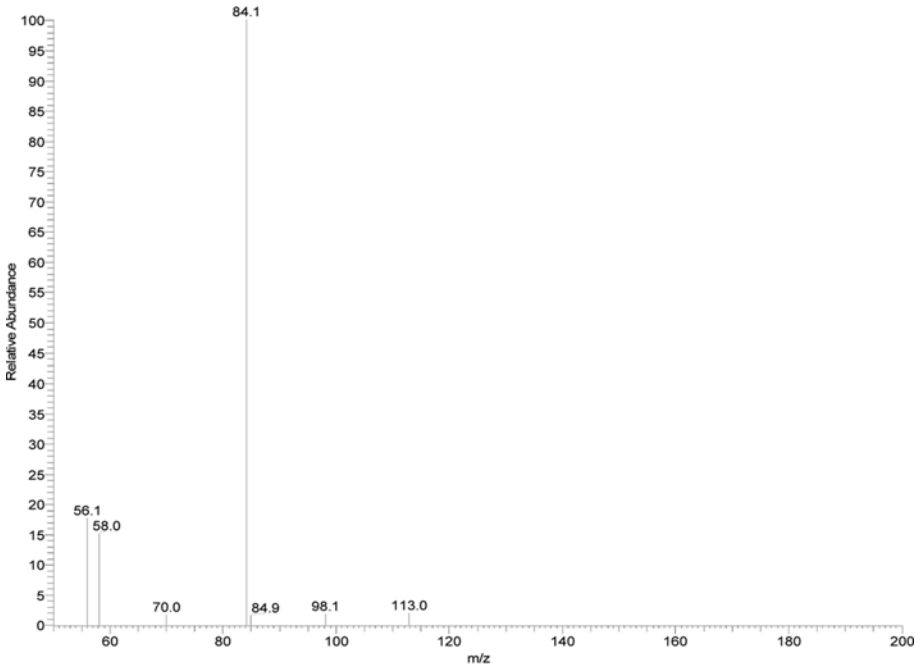

Fig. 7. Continued.

trum with a molecular weight of 200 or higher were assumed to originate from AEP urea formation, but this molecular weight was not observed in ^{13}C NMR; thus, only trace levels must have formed. Therefore, AEP urea formation was excluded from the reaction products. From the MS/MS and MS/MS/MS analysis results, skeletal structure fragmentation was observed as illustrated in Figs. 7 and 8. The free AEP fragment split ($[AEP+H]^+$=130.2) using the 120-200 m/z scan method is shown Fig. 7(a). The free AEP fragment splits clearly appeared in the MS/MS (Fig. 7(b)) and MS/MS/MS experiments (Fig. 7(c)). First, a $[AEP-NH_3+H]^+$=113.0

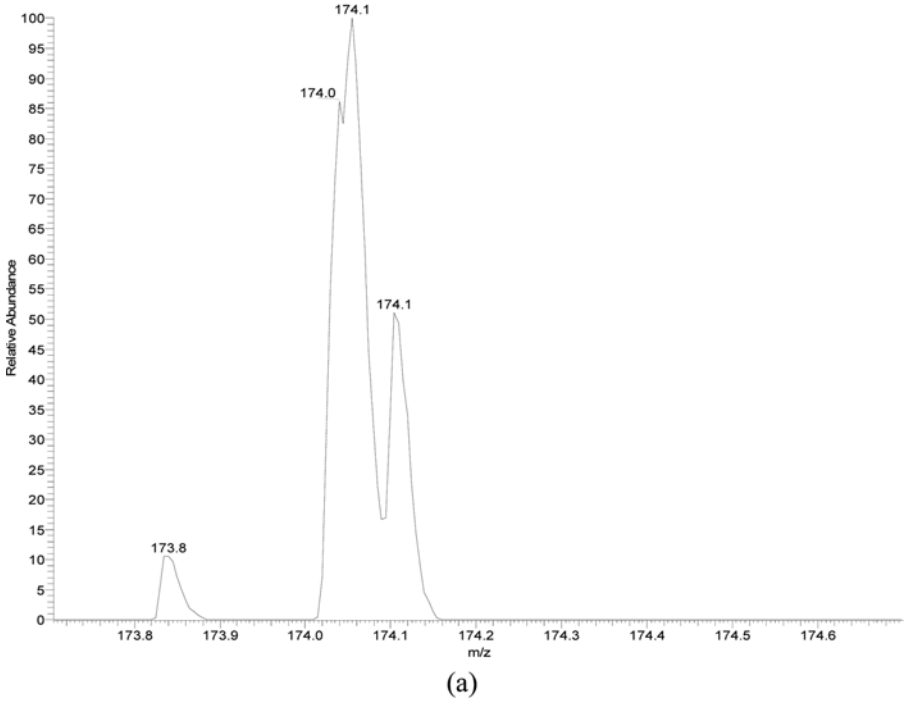

Fig. 8. Separation pattern of carbamate in a CO_2-saturated AEP solution: (a) $[AEP+CO_2+H]^+$=174.1 (MS), (b) $[AEP+H]^+$=130.1 (MS/MS) and (c) $[AEP-NH_3+H]^+$=113. 0 (MS/MS/MS).

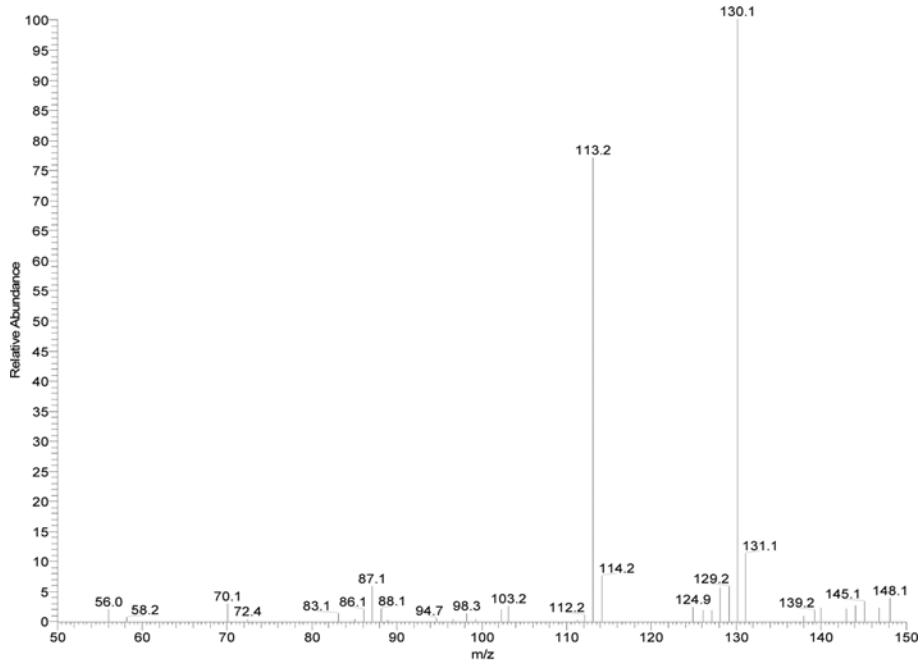

(b)

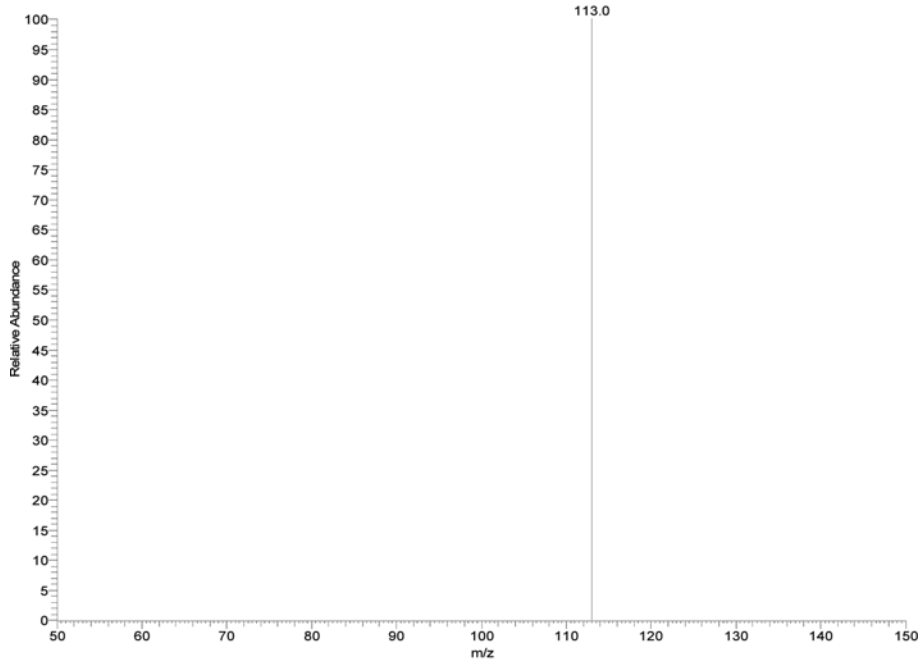

(c)

Fig. 8. Continued.

peak is shown in Fig. 7(b) as an amino group in the separated free AEP. Second, $[AEP\text{-}NH_3\text{-}2CH_3+H]^+$=84 is also shown in Fig. 7(c) as two methyl groups at $[AEP\text{-}NH_3+H]^+$=113.0, which were separated. Therefore, the free AEP was assigned to the 130.2 m/z peak in the MS analysis. The $[AEP+CO_2+H]^+$=174.1 peak in Fig. 8(a) was analyzed using the same method. A CO_2 molecule in $[AEP+CO_2+H]^+$=174.1 is easily separated under the MS ion conditions. As a result, $[AEP+H]^+$=130.1 and $[AEP\text{-}NH_3+H]^+$=113.0 fragment splits appeared in Fig. 8(b) and Fig 8(c), respectively. The MS results confirm that the reaction between CO_2 and AEP formed AEP carbamate, which is consistent with the NMR results.

CONCLUSIONS

The CO_2 absorption characteristics of an aqueous AEP solution, which features primary, secondary, and tertiary amino groups, were studied by comparing the solution to the representative commercial amine, MEA. The results at 333.15 K showed that AEP

exhibits 2.2-fold greater CO_2 loading than MEA. The apparent absorption rate for AEP was similar to DEA. Further, NMR and MS analysis methods were used to confirm the behavior of an aqueous AEP solution when it absorbed CO_2. The experimental results show that AEP exhibits all the characteristics of primary, secondary, and tertiary amines. However, interestingly, a bicarbamate of AEP did not form, and AEP-1-carbamate or AEP-7-carbamate was selectively formed. At the high CO_2 loading, bicarbonate was formed. Three different amino groups in the AEP reacted with CO_2 in following the order: primary>secondary>tertiary. The AEP exhibited excellent CO_2 absorption characteristics, including CO_2 loading and the absorption rate. Furthermore, AEP also exhibited high stability for thermal degradation compared with MEA [18]. Therefore, AEP could be expected to replace MEA as an absorbent. However, additional researches are still needed to replace the absorbent as physical properties, oxidative degradation, nitrosamine formation, foaming potential, mass transfer under absorber conditions and CO_2 cyclic capacity.

ACKNOWLEDGEMENTS

This work was supported by the Energy Demand Management Technology Program of the Korea Institute of Energy Technology Evaluation and Planning (KETEP), granted financial resource from the Ministry of Trade, Industry and Energy, Republic of Korea (No. 20152010201940).

REFERENCES

1. A. Albo, P. Luis and A. Irabin, *Ind. Eng. Chem. Res.*, **49**, 11045 (2010).
2. G. Marland, T. A. Boden and R. J. Andres, Global, regional, and national CO_2 emissions, Trends: A compendium of data on global change, Statistical Review of World Energy (2010).
3. R. Allam and O. Bolland, IPCC special report: Carbon dioxide capture and storage, IPCC Working Group III (2005).
4. R. Thiruvenkatachari, S. Su, H. An and X. X. Yu, *Prog. Energy Combust. Sci.*, **35**, 438 (2009).
5. A. J. Applehy and F. R. Foulkes, Fuel Cell Handbook, Van Nostrand Reinhold, New York (1989).
6. C. Han, K. Graves, J. Neathery and K. Liu, *Energy Environ. Res.*, **1**, 67 (2011).
7. Y. E. Kim, J. H. Choi, S. C. Nam and Y. I. Yoon, *Ind. Eng. Chem. Res.*, **50**, 9306 (2011).
8. J. Davison, *Energy*, **32**, 1163 (2007).
9. F. Closmann, T. Nguyen and G. T. Rochelle, *Energy Procedia.*, **1**, 1351 (2009).
10. D. Singh, E. Croiset, P. L. Douglas and M. A. Douglas, *Energy Convers. Manage.*, **44**, 3073 (2003).
11. R. Davy, *Energy Procedia*, **1**, 885 (2009).
12. M. H. Li and K. P. Shen, *Fluid Phase Equilib.*, **85**, 129 (1993).
13. M. D. Cheng, A. R. Caparanga, A. N. Soriano and M. H. Li, *J. Chem. Thermodyn.*, **742**, 342 (2010).
14. F. Y. Jou, A. E. Mather and F. D. Otto, *Can. J. Chem. Eng.*, **73**, 140 (1995).
15. A. Veawab, P. Tontiwachwuthikul and A. Chakma, *Ind. Eng. Chem. Res.*, **38**, 3917 (1999).
16. A. Veawab, P. Toniwachwuthikul and S. D. Bhole, *Ind. Eng. Chem. Res.*, **1**, 36 (1997).
17. P. Singh, D. W. F. Brilman and M. J. Groeneveld, *Energy Procedia*, **1**, 1257 (2009).
18. Y. Du, L. Li, O. Namjoshi, A. K. Voice, N. a. Fine and G. T. Rochelle, *Energy Procedia.*, **37**, 1621 (2013).
19. Y. Du and G. T. Rochelle, *Energy Procedia*, **63**, 997 (2014).
20. R. Zhang, E. P. Bonnin-Nartker, G. A. Farthing, L. Ji, M. G. Klidas, M. E. Nelson and L. M. Rimpf, *Energy Procedia.*, **4**, 1660 (2011).
21. Y. Zhang, *Ind. Eng. Chem. Res.*, **50**, 163 (2011).
22. P. Jackson, K. J. Fisher and M. I. Attalla, *Am. Soc. Mass. Spectrom.*, **22**, 1420 (2011).
23. M. S. Islam, R. Yusoff and B. S. Ali, *Engineering e-Transaction.*, **2**, 97 (2010).
24. M. Caplow, *J. Am. Chem. Soc.*, **90**, 6795 (1968).
25. P. V. Danckwerts, *Chem. Eng. Sci.*, **34**, 443 (1979).
26. H.-B. Xie, Y. Zhou, Y. Zhang and J. K. Johnson, *J. Phys. Chem. A.*, **114**, 11844 (2010).
27. F. Barzagli, F. Mani and M. Peruzzini, *Energy Environ. Sci.*, **2**, 322 (2009).
28. A. K. Chakraborty, K. B. Bischoff, G. Astarita and J. R. Damewood, Jr., *J. Am. Chem. Soc.*, **110**, 6947 (1988).
29. D. Prakash, E. Vaidya and Y. Kenig, *Chem. Eng. Technol.*, **30**, 1467 (2007).
30. F. Barzagli, F. Mani and M. Peruzzini, *Inter. J. Greenhouse Gas Control*, **5**, 448 (2011).
31. C. Perinu, B. Arstad and K.-J. Jens, *Int. J. Greenhouse Gas Control*, **20**, 230 (2014).
32. J. H. Choi, S. G. Oh, Y. E. Kim, Y. I. Yoon and S. C. Nam, *Environ. Eng. Sci.*, **29**, 328 (2012).
33. I. H. Um, M. J. Kim, J. S. Min and D. S. Kwon, *Bull. Korean Chem. Soc.*, **15**, 523 (1997).
34. J. H. Choi, S. G. Oh, Y. I. Yoon, S. K. Jeong, K. R. Jang and S. C. Nam, *J. Ind. Eng. Chem.*, **18**, 568 (2012).
35. A. F. Ciftja, A. H. Hartono and H. F. Svendsen, *Int. J. Greenhouse Gas Control*, **16**, 224 (2013).